Single particle demultiplexer based on domain wall conduits

A. Torti, V. Mondiali, A. Cattoni, M. Donolato, E. Albisetti et al.

Additional information on Appl. Phys. Lett.
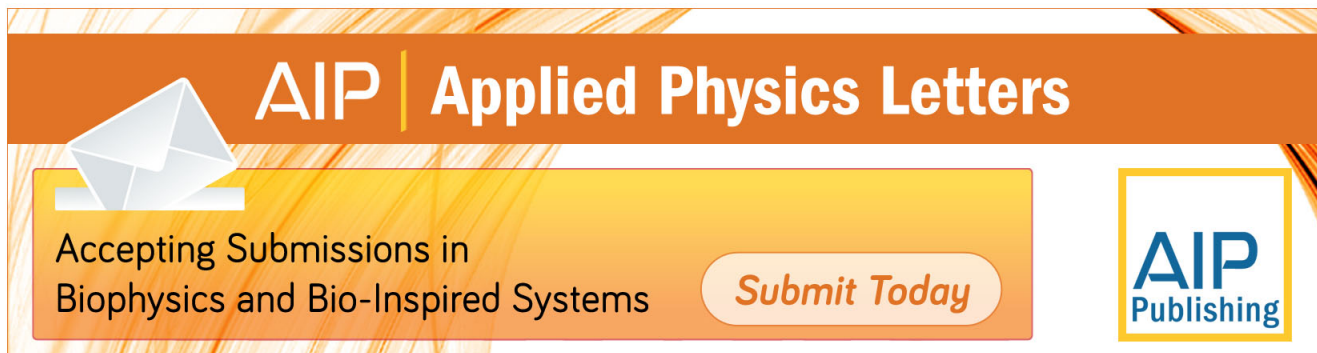
Single particle demultiplexer based on domain wall conduits

A. Torti,[1] V. Mondiali,[1] A. Cattoni,[2] M. Donolato,[3] E. Albisetti,[1] A. M. Haghiri-Gosnet,[2] Paolo Vavassori,[3,4] and R. Bertacco[1]

[1]*LNESS and CNISM, Dipartimento di Fisica, Politecnico di Milano, Via Anzani 42, 22100 Como, Italy*
[2]*Laboratoire de Photonique et de Nanostructures, Route de Nozay, 91460 Marcoussis, France*
[3]*CIC nanoGUNE Consolider, Tolosa Hiribidea 76, San Sebastian 20009, Spain*
[4]*IKERBASQUE, Basque Foundation for Science, Bilbao 48011, Spain*

The remote manipulation of micro and nano-sized magnetic particles carrying molecules or biological entities over a chip surface is of paramount importance for future on-chip applications in biology and medicine. In this paper, we present a method for the on-chip demultiplexing of individual magnetic particles using bifurcated magnetic nano-conduits for the propagation of constrained domain walls (DWs). We demonstrate that the controlled injection and propagation of a domain wall in a bifurcation allow capturing, transporting, and sorting a single magnetic particle between two predefined paths. The cascade of n levels of such building blocks allows for the implementation of a variety of complex sorting devices as, e.g., a demultiplexer for the controlled sorting among 2^n paths. © 2012 American Institute of Physics. [http://dx.doi.org/10.1063/1.4755785]

Conventional microfluidics is based on the transport of bio-entities fluid borne along predefined paths in a system designed for accomplishing different tasks in biological, medical, or chemical applications.[1] Another approach is however possible, based on the motion induced by forces directly applied on such entities within a fluid in static conditions. In this perspective, the use of magnetic particles as carriers of molecules or cells[2] benefits from the advantage of their easy manipulation via application of external magnetic field gradients, which are not screened by common fluids. Currently available methods, generally based on the application of external non-uniform magnetic fields,[3] are well suited for activating the motion of large populations of magnetic particles, while the controlled manipulation at the level of the single particle requires different strategies. Recently, the use of domain walls (DWs) in magnetic conduits patterned on a chip has been proved to be a viable path to achieve highly controllable motion of single micro and nanoparticles, with spatial resolution down to 100 nm. In addition, using the same approach, relatively high transport speed (up to several mm/s) has been demonstrated.[4–8] The method has been applied to the manipulation of both biomolecules[4] attached to a magnetic carrier and cells decorated with magnetic particles.[9] While transportation of a single bead by DWs along a line has been demonstrated in several ways, more complex functionalities like sorting have not yet been achieved. On-chip magnetic sorting of individual bio-entities is a very hot topic since it would provide a versatile, non-invasive and highly biocompatible approach.[10–21] In this paper, we demonstrate the sorting of an individual magnetic bead at a bifurcation of a DW nano-conduit. The underlying physics as well as the impact of the design parameters is carefully analyzed experimentally and via micromagnetic calculations to provide the key guidelines for adapting this magnetic demultiplexing unit to different geometries and particle sizes.

The layout of the magnetic demultiplexing unit designed for the present study is shown in the scanning electron microscopy (SEM) image of Fig. 1(a). It consists of four different

portions: *(red)* a DW injector, constituted by an initial pad having a width of 500 nm, allowing for the creation of a single DW; *(green)* a zig-zag shaped conveyor structure with a tapered end to transport the DW towards the bifurcation and then annihilate it; *(yellow)* a curved sorting structure with a curvature radius of 7.5 μm; *(blue)* two separated zig-zag conduits tilted by $\pm 5°$ with respect to the horizontal direction, representing the two output lines of the demultiplexer. The tilt has been introduced to provide a geometrical way to achieve a larger spatial separation of the two ends of the output lines. The thickness of the conduits, made of Permalloy ($Ni_{80}Fe_{20}$), is 25 nm. Each segment of the zig-zag is 2 μm long while the conduits width is 250 nm. The distance between the last corner of the conveyor and the middle point of the curved structure is 2 μm.

Figs. 1(b)–1(e) show the magnetic force microscopy (MFM) images of the different portions of the demultiplexer unit upon application of the external magnetic field pulses used to operate the device. The structure is initialized by applying a pulsed field $\mu_0\mathbf{H_0}$ of 50 mT along the negative x-direction, as shown in Fig. 1(b). Only a DW is present at the beginning of the bifurcation, displayed as a dark spot in the MFM image.[22] Subsequently, a head-to-head (HH) DW is injected by applying a momentary injection field $\mu_0\mathbf{H_i}$ of 14 mT, as in Fig. 1(c), which reverses the magnetization of the injection pad and propagate the DW up to the first corner in the zig-zag. The DW position remains stable after removal of $\mathbf{H_i}$, due to geometrical pinning potential at the corner. This is the position at which the DW captures a magnetic particle in suspension. As described in a previous work,[4] the DW and the captured magnetic bead can now be displaced along the conduit up to the last corner of the conveyor, with a sequence of external magnetic field pulses $\mu_0\mathbf{H_{up}}$ and $\mu_0\mathbf{H_{dw}}$ of 16 mT, at $\pm 45°$ with respect to the x-direction. By applying a field $\mu_0\mathbf{H_{bif}}$ of 31 mT along the positive x-direction, the DW (dashed arrow in Figs. 1(d) and 1(e)) on the last corner is annihilated and simultaneously another DW is created in the curved segment making the bead jump from
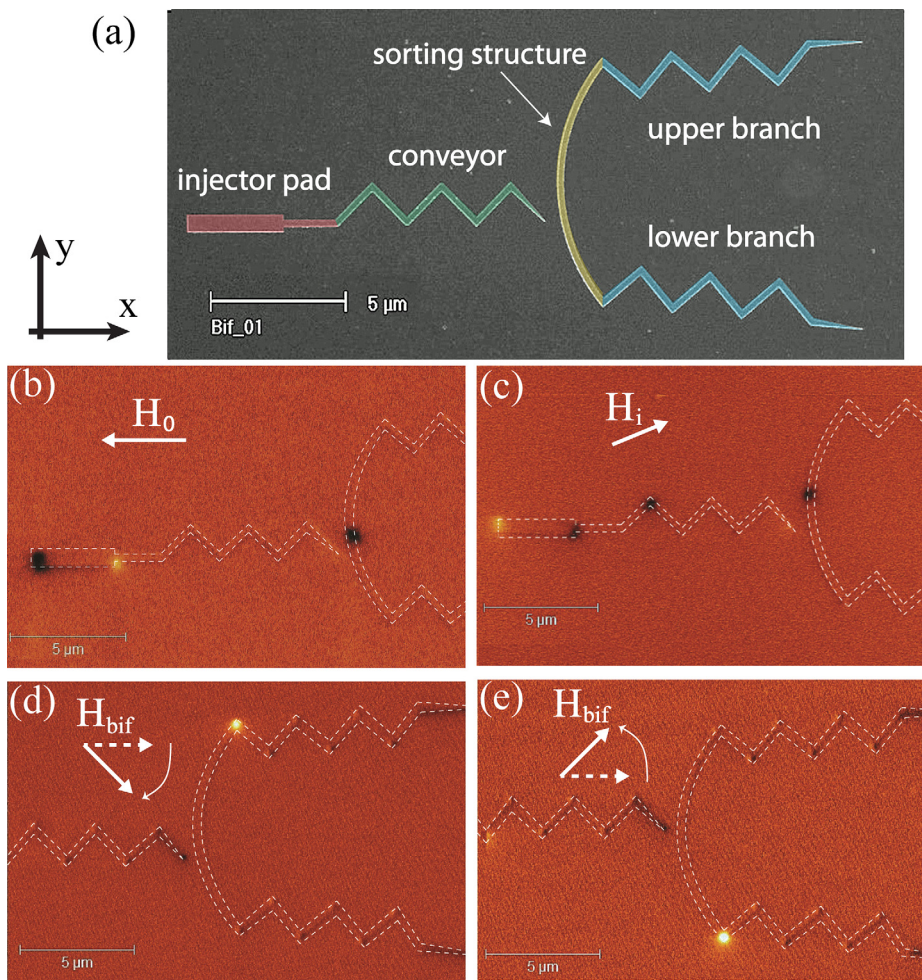
  101, 142405-1

FIG. 1. (a) False coloured SEM micrograph of the Py structure, 25 nm thick. The minimum distance between the tapered end of the conveyor and the bifurcated structure is 300 nm. (b)–(e) MFM images of the micromagnetic configurations after the application and removal of the sketched magnetic field. White dashed lines show the outline of the magnetic structures. Dark and bright spots are, respectively, HH and TT DWs. Spots at the injector pad are not due to DWs.

the conveyor to the bifurcation (not shown for space reasons). In this way, the zig-zag structures of the conveyor and the output branches are driven in a single domain configuration, while a tail-to-tail (TT) DW is nucleated at the middle point of the curved structure of the bifurcation. The external field is then kept constant in intensity and continuously rotated by 60° clockwise or counterclockwise with respect to the x-axis in order to displace the DW to the first corner of the upper or lower branch, respectively. The presence of a single TT DW at the first upper (lower) corner of the bifurcated structure is shown in Figs. 1(d) and 1(e) after the application of the rotating field (bright spot in Figs. 1(d) and 1(e)). Note that $\mathbf{H_{bif}}$ does not cause the nucleation of additional DWs in the structure. Once the DW is stabilized at the initial corner of the selected output branch, $\mathbf{H_{bif}}$ is removed and the TT DW propagates along the zig-zag upon application of the same sequence of field pulses used in the conveyor conduit but reversing their sign due to the polarity of the propagating TT DW, which is opposite to that of the initial HH DW in the conveyor. The change in the polarity of the propagating DW (from HH to TT) has no effect on the manipulation of magnetic beads in suspension over the conduit: a superparamagnetic bead is attracted by the DW stray field independently of the DW type.

In order to analyze in detail the micromagnetic behavior of the magnetic demultiplexing unit, simulations of DW motion in the arched sorting structure induced by a rotating field have been carried out with the OOMMF platform.[23]

The radius and width of the arch were varied in order to determine the threshold value ($\mu_0\mathbf{H_{th}}$) of the field ($\mu_0\mathbf{H_{bif}}$) required to achieve a continuous and robust motion. Frames of a video of the simulated DW motion in an arched structure induced by a rotating field is available in the supplementary material,[24] where we report also the parameters used in the simulations. The intensity of this magnetic field must be below a critical value of 50 mT in order not to nucleate other DWs in the two zig-zag shaped output lines. Keeping the width fixed at 250 nm, we found only a slight increase of $\mu_0\mathbf{H_{th}}$, from 35 to 40 mT, when the curvature radius of the arch increases from 7.5 μm to 25 μm. The DW spin structure is also not sizably affected by changes in the curvature radius for a constant width. This opens the possibility to employ arches with radius of tens of microns, which could be desirable for increasing the distance between the output lines of the demultiplexing unit in sorting applications. On the other hand, the arch width (w) is a much more critical parameter. In Fig. 2, we report the values of $\mu_0\mathbf{H_{th}}$ (dashed line–empty dots) and of the vertical force (F_z) (solid lines-filled dots) on typical superparamagnetic beads (magnetic susceptibility $\chi = 0.39$) of variable diameter ranging from 100 nm to 1 μm, and for arches with w ranging from 100 nm to 400 nm: The curvature radius of the arched structure is fixed to 7.5 μm. When increasing w, a sizable decrease of $\mu_0\mathbf{H_{th}}$ is seen, from 60 mT to 25 mT, thus, suggesting the choice of a large width for an easy displacement of a DW. However, the force on a bead coupled to the DW also depends on w, with different
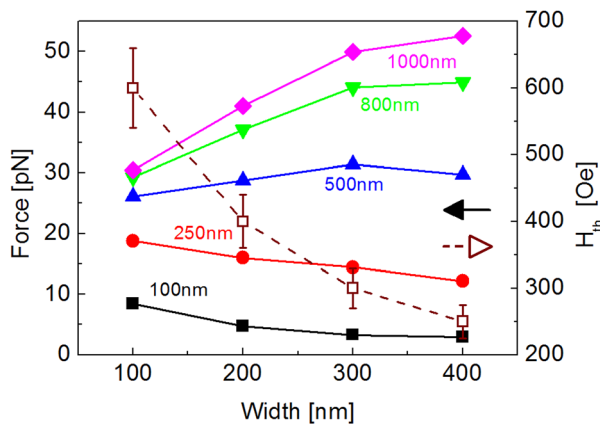
FIG. 2. (dashed line and empty dots) Threshold values (H_{th}) for the rotating magnetic field producing a robust wall motion in the curved conduit, as a function of the conduit width. (full dots) Magnetic force on a superparamagnetic bead having $\chi = 0.39$ and diameter ranging from 100 nm to 1 μm, versus the conduit width. The force is calculated for a bead with the bottom surface placed 50 nm above the magnetic conduit.

trends depending on the bead diameter. This is clearly visible in Fig. 2, showing that for beads with a diameter below 250 nm F_z decreases as w increases, while the opposite occurs for beads with diameter of 500 nm or bigger. This marked difference can be explained with reference to the transition of the spin configuration of the DW in the arch (25 nm thick), which is transverse for $w = 100$ nm and becomes vortex-like at about $w = 400$ nm. This transition of the internal spin structure of the DW and the corresponding increase of the DW extension produce a spreading of the magnetic charges (attracting poles) associated to the DW, which results in a decrease of the force on a particle much smaller than the DW spatial extension. On the other hand, the force on a bead with dimension comparable to that of the vortex-like DW, can beneficiate of such spreading of the attracting poles since a bigger portion of its volume will experience a sizable specific force.[9] As a key

result, this analysis demonstrates that the coupling force can be finely tailored by choosing the most appropriate w for the size of the beads to be sorted.

A key part of the design of the device is the gap between the conveyor and the middle point of the arched sorting structure, where the trapped bead has to jump across. Physically joining the two parts is not an option since simulations and experiments carried out on conduits, where the conveyor is connected to the curved segment, showed that a sizable remnant stray field originates at the bifurcation point, which disturbs and eventually prevents a reliable propagation of a bead captured by the DW along the arched conduit. In addition, the unavoidable asymmetry of the zig-zag conveyor with respect to the x axis determines a preferential motion of the DW towards one (the closest) of the two output lines of the demultiplexer. The gap allows for the circumvention of this problem. The application of H_{bif} along the x axis produces the simultaneous annihilation of the HH DW, previously at the last corner of the conveyor (state A), and the nucleation of a second TT DW at the center of the arch (state B). The annihilation is achieved by tapering the end of the conveyor. Furthermore, a gap of 2 μm allows magnetic beads, at least with a diameter of 500 nm, to safely follow the next DW equilibrium position.[4]

The calculated spin configuration and magnetic potential energy of a 1 μm diameter bead with the bottom surface at 50 nm height from a Py conduit having width of 250 nm (i.e., at the typical distance of a bead in contact with the 50 nm thick SiO_2 capping layer we used in experiments), are shown in Figs. 3(a) and 3(c) for states A and B, respectively. The corresponding values of the vertical component of the force (F_z) acting on the bead placed above the conduit are reported in Figs. 3(b) and 3(d). The force vector field ($\mathbf{F}$) and the F_z felt by the bead has been computed in a MATLAB script by taking the gradient of the magnetic potential energy (E_b): $\mathbf{F} = -\nabla E_b$. The magnetic potential energy of a bead above a DW has been
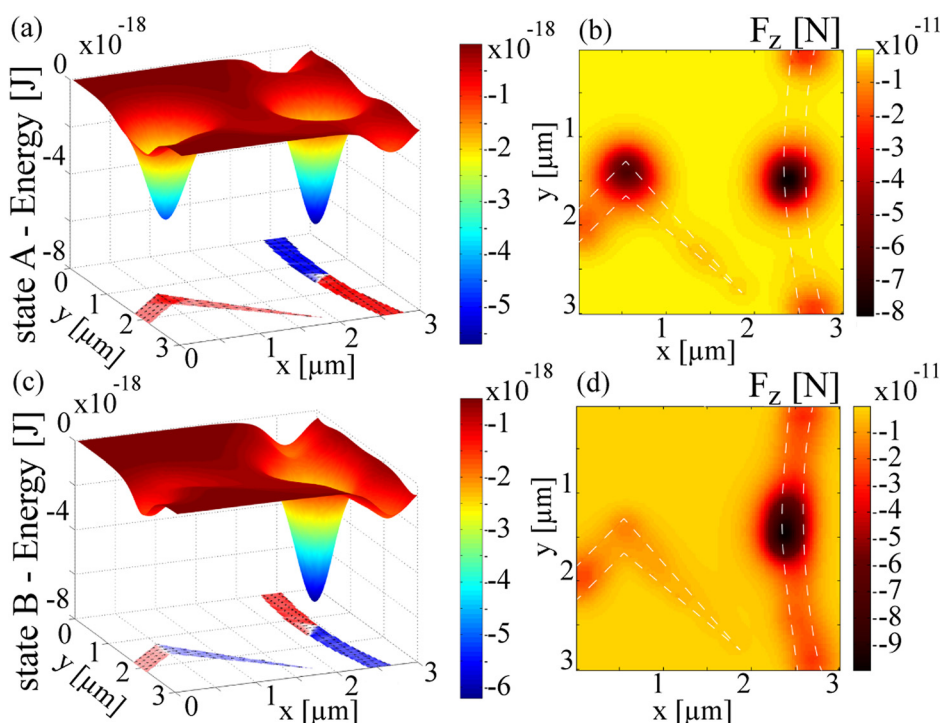

FIG. 3. (a) Magnetic potential energy of 1 μm diameter bead (sphero^{TM}) when the injected DW is at the last corner of the conveyor (state A). The bottom surface of the bead is at 50 nm height above the Py conduit. (b) Contour plot of the vertical force (F_z) generated by the potential shown in (a). The dotted white lines depict the edges of the magnetic conduits. (c) Magnetic potential energy upon application of an external field $\mu_0 H_{bif}$ of 30 mT (state B). (d) Contour plot of the vertical force generated by the magnetic configuration in state B.

calculated by integrating the Zeeman energy density over the particle volume: $E_b = -\mu_0 \chi \int_{Vb} \mathbf{H_{dw}} \cdot \mathbf{H_{dw}} dV$. In state B, the simulations have been carried out with $\mathbf{H_{bif}}$ applied. The vertical force on a bead at the equilibrium position above the last corner of the conveyor is on the order of 80 pN. When $\mathbf{H_{bif}}$ is applied, we obtain only one pronounced potential well at the middle of the arch created by the subsequent TT DW. The fringing field at the tapered end of the conveyor is minimized since the magnetic charges are distributed over a large surface. The vertical force produced there on a 1 μm bead is below 10 pN, while at the bifurcation is $\sim$100 pN.

Experiments, which results are shown in Fig. 4, confirm the behavior expected from the simulations and the sorting of beads with different diameters has been demonstrated using the demultiplexer unit structure shown in Fig. 1(a). The extension of the conveyor and of the two output branches of the device used to illustrate the working principle of the unit are 12 μm and 10 μm, respectively, but there is no fundamental limitation to the length of these zig-zag shaped conduits. The operation of the device has been tested with 1 μm (sphero^{TM})
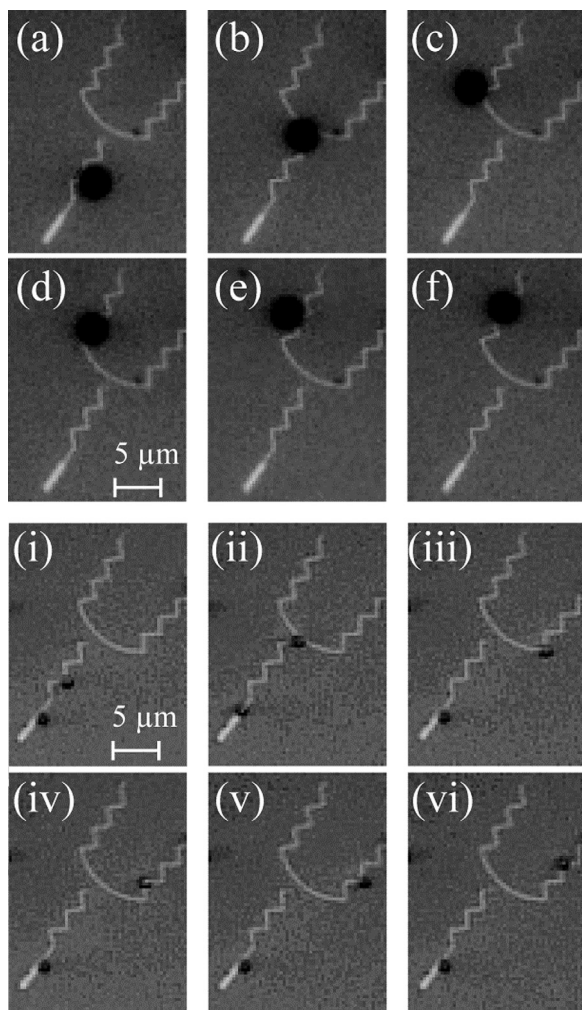

FIG. 4. (a)–(f) Sequence of frames from Video 1 showing the transport to the bifurcation and the sorting to the upper branch of a 2.8 μm magnetic bead coated with streptavidin. (i)–(vi) Sequence of frames from Video 2 showing the transport to the bifurcation and the sorting to the lower branch of a 1 μm magnetic bead. See supplementary material for full captions for Videos 1 and 2 (Ref. 24); (enhanced online) Video 1 [URL: http://dx.doi.org/10.1063/1.4755785.1], Video 2 [URL: http://dx.doi.org/10.1063/1.4755785.2].

and 2.8 μm (Dynabeads$^{®}$ M-280) diameter beads, which allow for an easier real-time monitoring of the bead motion by optical microscopy.[24] The sequence of frames reported in Fig. 4 shows the remotely controlled displacement and sorting to the upper or lower output line of the demultiplexer of individual 2.8, panels (a)-(f) (see Video 1), and 1 μm beads, panels (i)-(vi) (see Video 2). Once the HH DW is nucleated in the first corner of the conveyor a suspension of beads with a concentration of 10^6 particles/μl is flushed in the microfluidic cell placed in a quadrupolar electromagnet under the microscope. When a bead is captured by the HH DW [Figs. 4(a) and 4(i)], the flow is stopped and we start the manipulation procedure by applying a sequence of alternating fields at $\pm 45°$ with respect to the long axis of the structure to propagate the DW coupled to the bead. Once the bead is on the last corner of the conveyor, a magnetic field $\mu_0 \mathbf{H_{bif}}$ of 33 mT along the long axis (x direction) annihilates the HH DW and the bead jumps from the conveyor to the middle point of the sorting structure where the second TT DW is nucleated [Figs. 4(b), 4(c), 4(ii), and 4(iii)]. The minimum value of $\mu_0 \mathbf{H_{bif}}$ ensuring the jump is greater than the one found by MFM by about 2 mT. This can be qualitatively explained by the coupling between the DW and the particle that deepens the pinning potential well for the DW at the corner.[25] By rotating $\mathbf{H_{bif}}$ from 0° to $\pm 60°$, the particle is displaced to the upper or lower branch [Figs. 4(d), 4(iv)]. When the $\mathbf{H_{bif}}$ field is removed, the TT DW at the first corner of the selected output line structure is in a stable equilibrium state. By applying a series of magnetic field pulses, as for the conveyor conduit but reversing the sign, the particle is displaced along the zigzag conduit of the selected branch of the sorting unit [Figs. 4(e), 4(f), 4(v), and 4(vi)]. Finally the particle can be released at the end of the structure by annihilating the DW in the tapered end of the output line. This technological platform holds the potential for remotely controlling the propagation of single magnetic particle along a variable and arbitrarily complex path since its design allows for adding a sorting structure at the end of each branch. As an example, the cascade of *n* levels of such building blocks allows for the implementation of a demultiplexer for the controlled sorting among 2^n paths.

To summarize, in this paper we demonstrated the on-chip sorting of individual magnetic particles in suspension using a bifurcated domain wall conduit. Detailed micromagnetic simulations have been used to guide the optimization procedure and to interpret experimental results. The sorting of micrometer sized particles has been demonstrated but the method can be applied also to nanometer sized particles.

[1]H. Bruus, *Theoretical Microfluidics* (Oxford University Press, Oxford, 2008).

[2]Y. Pan, X. Du, F. Zhao, and B. Xu, Chem. Soc. Rev. **41**, 2912 (2012).

[3]M. A. M. Gijs, Microfluid. Nanofluid. **1**, 22 (2004).

[4]M. Donolato, P. Vavassori, M. Gobbi, M. Deryabina, M. F. Hansen, V. Metlushko, B. Ilic, M. Cantoni, D. Petti, S. Brivio, and R. Bertacco, Adv. Mater. **22**, 2706 (2010).

[5]E. Rapoport and G. S. D. Beach, Appl. Phys. Lett. **100**, 082401 (2012).

[6]T. Ono, H. Miyajima, K. Shigeto, K. Mibu, N. Hosoito, and T. Shinjo, Science **284**, 468 (1999).

[7]D. A. Allwood, G. Xiong, C. C. Faulkner, D. Atkinson, D. Petit, and R. P. Cowburn, Science **309**, 1688 (2005).

[8]P. Vavassori, V. Metlushko, B. Ilic, M. Gobbi, M. Donolato, M. Cantoni, and R. Bertacco, Appl. Phys. Lett. **93**, 203502 (2008).

[9]M. Donolato, A. Torti, N. Kostesha, M. Deryabina, E. Sogne, P. Vavassori, M. F. Hansen, and R. Bertacco, Lab Chip **11**, 2976 (2011).

[10]A. Y. Fu, H. Chou, C. Spence, F. H. Arnold, and S. R. Quake, Anal. Chem. **74**, 2451 (2002).

[11]A. Lenshof and T. Laurell, Chem. Soc. Rev. **39**, 1203 (2010).

[12]A. Ashkin, Proc. Natl. Acad. Sci. U.S.A. **94**, 4853 (1997).

[13]M. C. Wu, Nat. Photonics **5**, 322 (2011).

[14]S. Fiedler, S. G. Shirley, T. Schnelle, and G. Fuhr, Anal. Chem. **70**, 1909 (1998).

[15]B. B. Yellen, R. M. Erb, H. S. Son, Jr., H. Rodward, H. Shang, and G. U. Lee, Lab Chip **7**, 1681 (2007).

[16]S. Miltenyi, W. Müller, W. Weichel, and A. Radbruch, Cytometry **11**, 231 (1990).

[17]N. Pamme, Lab Chip **7**, 1644 (2007).

[18]A. Ehresmann, D. Lengemann, T. Weis, A. Albrecht, J. Langfahl-Klabes, F. Göllner, and D. Engel, Adv. Mater. **23**, 5568 (2011).

[19]M. Donolato, B. T. Dalslet, and M. F. Hansen, Biomicrofluidics **6**, 024110 (2012).

[20]G. Vieira, T. Henighan, A. Chen, A. J. Hauser, F. Y. Yang, J. J. Chalmers, and R. Sooryakumar, Phys. Rev. Lett. **103**, 128101 (2009).

[21]P. Tierno, S. V. Reddy, M. G. Roper, T. H. Johansen, and T. M. Fischer, J. Phys. Chem. B. **112**, 3833 (2008).

[22]Dark and bright portions at the injector pad are not DWs but they are due to the stray field of the two edges.

[23]M. J. Donahue and D. G. Porter, Interagency Report NISTIR 6376, 1999.

[24]See supplementary material at http://dx.doi.org/10.1063/1.4755785 for the experimental procedure.

[25]M. T. Bryan, J. Dean, T. Schrefl, F. E. Thompson, J. Haycock, and D. A. Allwood, Appl. Phys. Lett. **96**, 192503 (2010).